Baryon rapidity loss and midrapidity stacking in high energy nucleus-nucleus collisions

F. Videbæk
Department of Physics, Brookhaven National Laboratory, Upton, New York 11973

Ole Hansen
Niels Bohr Institute for Astronomy, Physics, and Geophysics, University of Copenhagen, DK-2100 Copenhagen Ø, Denmark

(Received 30 June 1995)

Rapidity distributions of baryons from nucleus-nucleus, p-nucleus, and p-p interactions at 11.6, 14.6, and 200 GeV/c per nucleon incident momenta are reviewed. Average rapidity losses relative to the beam rapidity are derived in a consistent way and the systematics are described and discussed. The baryon multiplicities in the midrapidity region relative to simple geometrical sum rules are determined and the systematics of the opacity of the collisions are described. The main conclusions are that the average rapidity losses in central nucleus-nucleus collisions scale with the projectile rapidity and that the opacity of central collisions depends strongly on the size of the collision system and weakly on incident momentum.

PACS number(s): 25.75.+r

I. INTRODUCTION

The physics of a fast moving particle penetrating extended matter has been widely studied. Bohr was among the first to describe systematically the stopping process of an atomic particle at velocity close to the speed of light (see, e.g., Refs. [1,2]). The approximations underlying the atomic stopping theory are (see, e.g., [3]) that the momentum transfer in each collision be small compared to the momentum of the impinging particle, that the identity and path of the projectile be well defined, and that the stopping matter is extended.

The physics of stopping in high energy nucleus-nucleus collisions is fundamentally different from the physics of atomic stopping, primarily because the main acting force is the strong force rather than the electromagnetic force. In nucleus-nucleus collisions the momentum transfer may be comparable to the momentum of the projectile; the concept of extended nuclear matter cannot be realized in the laboratory, so the extension of the projectile is often comparable to that of the stopping object; the momentum transfer in a collision is often comparable to the rest masses of the colliding particles, so the identity of the projectile is not secured, and the idea of a well defined path through the stopping matter has largely lost its validity.

Instead of using the kinetic energy loss per unit length (stopping power), as is done in atomic stopping, to characterize the process, following Daté *et al.* (Ref. [4]), the average rapidity loss of the projectile is adopted as the characteristic quantity, a quantity that can be defined in an operational way and is invariant under Lorentz transformations along the beam axis (boost invariant).

The incoming projectile direction is taken as the z axis, the total energy of a particle is denoted E, the magnitude of its momentum p, and the projection of the momentum on the beam axis p_z. The rapidity is then defined as

$$y=\frac{1}{2}\ln\frac{E+p_z}{E-p_z}. \tag{1}$$

The average rapidity loss is

$$\langle \delta y\rangle = y_p - \langle y_b\rangle, \tag{2}$$

where y_p is the incoming projectile rapidity and $\langle y_b\rangle$ is the average net baryon rapidity after the collision. Net baryons, i.e., the number of baryons minus the number of antibaryons, were chosen in order to count mainly leading baryons that are related to the incoming baryons and avoid counting created baryons (see also Sec. II A below).

In a symmetric collision, $p+p$ or $A+A$, the wave function of the colliding system is either symmetric or antisymmetric under the exchange of target and projectile. It is therefore not possible to distinguish baryons as originating from the target or from the projectile; one must deal with the collision system as a whole. The rapidity density (dn/dy) distribution is symmetric about midrapidity, $y_m=\frac{1}{2}y_p$, so the average net baryon rapidity $\langle y_b\rangle = y_m$. In order to evaluate $\langle \delta y\rangle$ from Eq. (2), the averaging is taken from y_m to $\approx y_p$ (or equivalently from y_m to ≈ 0). For an asymmetric collision system, A_1+A_2, the projectile baryons, in the limit of transparency (small $\langle \delta y\rangle$), can be distinguished from the target baryons, and the averaging over y_b then should be made for those baryons only which are related to the projectile, in analogy to the case of atomic stopping, where a light projectile is impinging upon an infinitely heavy, but thin target. If the collision system, conversely, is black, so that projectile and target nucleons after the collision are entirely mixed, the concept of "projectile baryons" is of little use. It is not possible to devise a fundamental recipe and the actual cases are dealt with in a somewhat *ad hoc* manner in Sec. II C.

The present report offers (Sec. II) a systematic compilation of $\langle \delta y\rangle$ for $p+p$, $A+A$, and A_1+A_2 collisions at beam momenta of 11.6, 14.6, and 200 GeV/c per nucleon, the momenta at which there exist $A+A$ and A_1+A_2 results. $p+A$ reactions have not been analyzed for $\langle \delta y\rangle$ determination because of a lack of appropriate data near $y=y_p$. (See, however, the discussions in the review paper of Busza and Ledoux [5].)

0556-2813/95/52(5)/2684(10)/$06.00

TABLE I. The inclusive baryon data. The symbol × means that the particle in the column heading was observed. The symbol [×] denotes that net protons were measured. For further details, see the text.

p_p (lab) A GeV/c	y_p (lab)	$\sqrt{s}$ n-n GeV/c^2	A_1+A_2	p	$\bar{p}$	Λ	$\bar{\Lambda}$	References
11.6	3.21	4.86	Au+Au	×				[8,9]
12.0	3.24	4.93	$p+p$	×		×		[10]
14.6	3.44	5.41	p+Be	×				[11]
			p+Al	×				[11]
			p+Cu	×				[11]
			p+Au	×				[11]
			Si+Al	×				[12]
			Si+Cu	×				[12]
			Si+Au	×				[12]
			Si+Pb	×				[13,14]
24.0	3.94	6.84	$p+p$	×		×		[10]
69.0	4.99	11.46	$p+p$	×				[15]
200.0	6.06	19.42	S+S	[×]		×	×	[16,17]
			S+Ag	[×]		×		[18]
			S+Au	[×]		×		[18]
205.0	6.08	19.66	$p+p$			×		[19]
300.0	6.46	23.76	$p+p$			×	×	[20]
400.0	6.75	27.43	$p+p$	×	×			[21]

The average number of net baryons per collision, observed in the midrapidity ($\frac{1}{2}y_p$) region after the collision is of special interest for the study of "hot and dense matter," because it has been conjectured that a phase transition from hadronic matter to a quark-gluon plasma (here, baryon rich) may take place, if the temperature and/or the density becomes large enough over a volume large compared to that of a hadron (see, e.g., [6,7]). One might choose the net baryon dn/dy measured at midrapidity as a characteristic quantity in this connection, but midrapidity does not have a well defined kinematic significance in asymmetric collisions. Rather, the rapidity region of interest is the region within which most of the created particles appear, because this reflects the region of highest density and temperature. We have chosen to sum the net baryon dn/dy distribution over the rapidity region in which the majority of the K^- or $\bar{\Lambda}$ particles are found, i.e., between the points of half maximum of the K^- or $\bar{\Lambda}$ dn/dy distribution. K^- and $\bar{\Lambda}$ were chosen because they are not created in associated, quasielastic processes but largely in midrapidity production [see also the discussion of Eqs. (5) and (6) below].

In order to compare systems of different sizes, it is convenient to express the summed net baryon dn/dy in units of the maximum number one could expect, i.e., in terms of a sum rule limit. The total number of baryons in the system before the collision A_1+A_2 constitutes such a limit; we have instead chosen a limit approximately equal to the maximum number of *participating* baryons, thereby putting asymmetric and symmetric collisions on a similar footing. The number of participating baryons is calculated from simple geometric models (see Sec. III) and the ratio of measured baryon multiplicity over the sum rule limit is denoted F_b.

Section IV presents a brief description and discussion of the systematics observed for $\langle \delta y \rangle$ and F_b.

II. AVERAGE RAPIDITY LOSSES

Before the collision the baryon rapidity distribution consists of two peaks, one centered near $y=0$ and one near $y=y_p$. After the collision the baryon rapidity distribution extends from somewhat below the target rapidity ($y=0$) to somewhat above the projectile rapidity, and it may have a complicated shape. The experiments have finite acceptances, so the rapidity distributions therefore are measured as averages over a large number of collisions selected by a common trigger. The collisions are sampled as a weighted average over a range of impact parameters, where neither the range nor the weighting are known quantitatively from the experiments. The task is to define which baryons after the collision are related to the incoming baryons and make sure to include all of them in the evaluation of $\langle \delta y \rangle$. The prescriptions devised vary from case to case ($p+p$, $A+A$, and A_1+A_2) as described below.

A. $p+p$ collisions

Table I gives an overview of the available data. The majority of the heavy ion data are at 14.6A and 200A GeV/c momenta at which there are no $p+p \rightarrow p+X$ results in the literature. It is therefore necessary to rely on scaling of nearby $p+p$ data in order to establish $p+p$ reference results at the heavy ion momenta. The scaling chosen is rapidity scaling (see, e.g., [22,23]),

$$dn/dy_1 = \frac{\langle n_1 \rangle}{\langle n_2 \rangle} \frac{y_{2p}}{y_{1p}} \, dn/dy_2, \tag{3}$$

where $\langle n_i \rangle$ is the multiplicity at beam rapidity y_{ip}. For protons we have taken $\langle n_1 \rangle / \langle n_2 \rangle = 1$ at all incident rapidities,

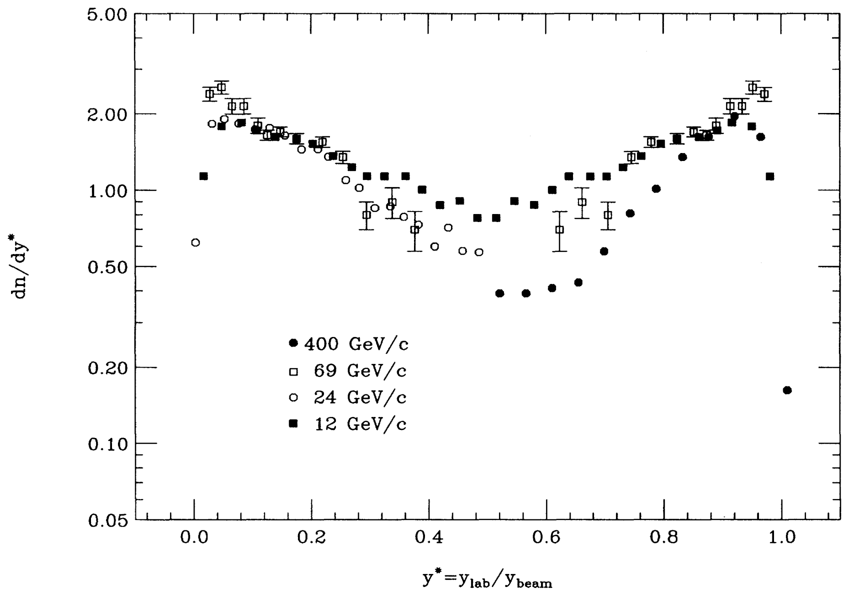

FIG. 1. The $p+p \rightarrow p+X$ rapidity densities dn/dy^* plotted as a function of $y^*=y/y_p$ [see Eq. (4)] at 12, 24, 69, and 400 GeV/c incident momenta. References are given in Table I.

while for Λ, $\bar{\Lambda}$, and $\bar{p}$ the $\sqrt{s}$ systematics of Wroblewski [24] were used. The Wroblewski $\sqrt{s}$ systematics are similar to the results in [25].

Equation (3) for protons implies that the density dn/dy^*, where

$$y^* \equiv y/y_p, \tag{4}$$

is independent of the incident momentum p_p. The measured proton dn/dy^* distributions are shown in Fig. 1 for incident momenta of 12, 24, 69, and 400 GeV/c. It is evident that the scaling law Eq. (3) is not quantitatively fulfilled. At midrapidity, $y^*=0.5$, the dn/dy^* decrease systematically with increasing p_p. At target and projectile rapidities the 12 and 24 GeV/c data agree well, so that scaling from 12 to 14.6 GeV/c will yield accurate $\langle y \rangle$ results. The establishment of 200 GeV/c data is more difficult. Table II shows the integrated dn/dy results from the data in Fig. 1 from $y=0$ to $y=1/2y_p$. The 69 GeV/c data have been extrapolated from the lowest y value measured ($y^*=0.65$) to midrapidity ($y^*=0.5$) by a constant value. The average multiplicities in the table are $\approx$0.60, except at 400 GeV/c, which has a markedly lower value. This is presumably caused by a high rapidity trigger inefficiency (see Ref. [21]), which can be corrected for only in an average way. The 69 GeV/c data have therefore been used to establish the 200 GeV/c reference dn/dy. The midrapidity extrapolation of the scaled 69 GeV/c results is of unknown accuracy, but plays a minor role for the $\langle y \rangle$ value.

TABLE II. Proton multiplicities in $p+p$ reactions.

p_p (lab) GeV/c	Multiplicity[a]	Comments
12	0.64±0.01	
24	0.58±0.01	
69	0.60±0.02	extrap.
40	0.48±0.01	

[a]The multiplicities are derived by summing $(dn/dy)\Delta y$ from target to midrapidity. The errors quoted are statistical only. The extrapolation is explained in the text.

The definition of $\langle \delta y \rangle$ in Eq. (2) refers to "net baryons." At 12 GeV/c the production of antibaryons is so low that there is no practical difference between net baryons and baryons. At 200 GeV/c the production of antibaryons may not be negligible. Antiprotons are produced by pair creation

$$N+N \rightarrow N+N+\bar{N}+N, \tag{5}$$

where the proton created in pair with the antiproton will appear near midrapidity. Such created protons are not leading protons and should not be counted in the evaluation of $\langle \delta y \rangle$. The antiproton dn/dy should therefore be subtracted from the proton dn/dy. The 200 GeV/c antiproton yield was constructed from the measured yield at 400 GeV/c by the scaling rule of Eq. (3). It may be noted that the high rapidity trigger inefficiency of the 400 GeV/c experiment mentioned above has negligible influence on the antiproton yields.

Λ particles may be created by associated production, an almost elastic process,

$$N+N \rightarrow N+\Lambda+K, \tag{6}$$

where K stands for a K meson. Λ particles produced in this way are leading baryons and they should be counted in the $\langle \delta y \rangle$ evaluation. There are Λ data at 205 GeV/c (see Table I) which have been used here without scaling. A Λ may also be created at midrapidity by pair creation together with a $\bar{\Lambda}$ [Eq. (5)] and such Λ's should be excluded. $\bar{\Lambda}$ yields have been measured at 300 GeV/c (see Table I) and scaled to 200 GeV/c. Figure 2 shows the Λ results at 205 GeV/c together with the 300 GeV/c Λ data scaled to 200 GeV/c. The agreement is good, but unfortunately there are no possibilities of testing antibaryon scaling for the incident momenta of interest here.

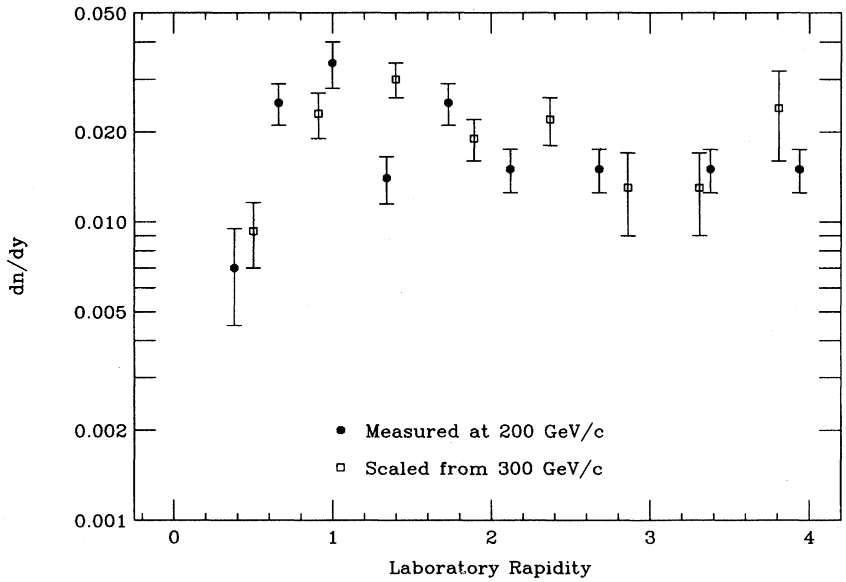

FIG. 2. $p+p \rightarrow \Lambda + X$ rapidity densities measured at 205 and 300 GeV/c in $p+p$ interactions. The 300 GeV/c data have been scaled to 205 GeV/c according to Eq. (3). Data references are given in Table I.

Table III shows the average rapidity value in the range $y^*=0.5$ to 1.0 for protons, protons minus antiprotons, and protons plus Λ's minus the corresponding antiparticles (named net all). The results for all three recipes agree within the statistical errors, so the choice of recipe is therefore not important.

Neutrons are created particles in $p+p$ interactions. They may be made by associated production (usually called charge exchange) by the near elastic process

$$p+p \rightarrow p+n+\pi^+ \tag{7}$$

in analogy to Eq. (6). If the center of mass momenta of the baryons are large compared to the π^+ mass, it may be assumed that the leading neutron dn/dy distribution is the same as the leading proton distribution, and hence that the neglect of the neutrons, for which we have not found any useful data, is of little consequence. Since the inclusion of Λ's did not affect the $\langle \delta y \rangle$ results, it may safely be assumed that the neglect of the heavier and more rare baryons is allowed.

The final 12, 14.6, and 200 GeV/c results for $\langle \delta y \rangle$ are given in Table IV, where protons have been used at the two lower energies and net all at 200 GeV/c.

TABLE III. Sensitivity of $\langle y_b \rangle$ to created baryons. The $p+p$ results are for a minimum bias trigger, while the $S+S$ data are from the cent-3 trigger (see Table IV).

System	p_p (lab)	$\langle y_b \rangle$	Part[a]
$p+p$	200 GeV/c	5.17±0.10	prot
		5.19±0.10	net prot
		5.18±0.10	net all
S+S	200A GeV/c	1.67±0.10	net prot
		1.69±0.10	net all

[a]Net protons means protons minus antiprotons and net all stands for protons plus Λ's minus the corresponding antiparticles.

B. Symmetric $A+A$ collisions

In heavy ion collisions it is customary to use triggers that distinguish between central and peripheral collisions. This is often done by using a calorimeter at zero degrees, that measures the kinetic energy of the part of the projectile that did not interact with the target and which therefore continued forward with the beam momentum per particle. Table V gives the average number of projectile nucleons that did participate in the collision, $\langle N_p^{\rm part} \rangle$, for the collision systems considered. The $\langle N_p^{\rm part} \rangle$ values were calculated from the measured average kinetic energy $\langle T_{z\rm cal} \rangle$ of the forward going projectile fragment, by

$$\langle N_p^{\rm part} \rangle = A_p \left(1 - \frac{\langle T_{z\rm cal} \rangle}{T_p} \right), \tag{8}$$

where T_p is the kinetic energy of the projectile and A_p the projectile mass number (see also [26]). Centrality triggers are characterized by the magnitude of the trigger cross section $\sigma_{\rm trig}$ relative to the inelastic cross section $\sigma_{\rm inel}$, and triggers with less than 10% of $\sigma_{\rm inel}$ are called central. Peripheral triggers have cross sections near 50%, as shown in the table.

While the centrality conditions on the average ensure a certain overlap between target and projectile, they do not select the centrality of the individual nucleon-nucleon interactions. If we take the nuclear radius to be $R=1.14A^{1/3}$ fm and the nucleonic radius as 0.8 fm, the average distance between nucleons is ≈2 fm, center to center. The $p+p$ inelastic cross section is 3 fm^2, corresponding to an interaction distance of 1 fm. A projectile nucleon in the projectile-target overlap region is thus in a situation where it may interact inelastically with some nucleon in the target and the individual N-N impact parameters will vary from zero to the interaction distance in some random fashion. Comparisons between central $A+A$ collisions and minimum bias $p+p$ interactions are thus not entirely unfair.

Figure 3 shows the net all dn/dy distribution for central (3%) S+S collisions in comparison with the net proton dis-

TABLE IV. Average projectile rapidity losses $\langle \delta y \rangle$. The average net baryon rapidity loss $\langle \delta y \rangle$ is given in column 3 for the collision systems shown in column 2 and the incident projectile momentum is noted in the first column. The multiplicity given in column 4 is the sum over $(dn/dy)\Delta y$ from target rapidity to midrapidity for the symmetric collision systems, and from beam rapidity to a rapidity $y_{\rm low}$ (given in the text) for the asymmetric systems. The baryons used in the evaluation are given in the next to last column. Net all is defined as protons plus Λ's minus the corresponding antiparticles, and net prot as protons minus antiprotons. The last column identifies the trigger conditions as shown in Table V. All uncertainties quoted are statistical only.

p_p (lab) A GeV/c	Collision	$\langle \delta y \rangle$	Multiplicity	Part	Trigger
12.0	$p+p$	0.71±0.01	0.64±0.01	prot	min
14.6	$p+p$	0.76±0.01	0.65±0.01	prot	min
200.0	$p+p$	0.89±0.10	0.62±0.02	net all	min
11.6	Au+Au	1.02±0.01	70.1±1.40	prot	cent-4
14.6	Si+Al	0.97±0.01	10.0±0.10	prot	cent-7
		0.79±0.01	2.3±0.10	prot	periph
200.0	S+S	1.69±0.10	14.2±0.70	net all	cent-3
		0.83±0.20	2.8±0.40	net prot	periph
14.6	Si+Au/Pb	1.33±0.01	13.65	prot	cent-7
		1.22±0.02	11.60	prot	cent-7
		1.44±0.02	13.80	prot	cent-2
		1.34±0.02	11.70	prot	cent-2

tribution from peripheral S+S interactions at 200A GeV/c. The distribution shape for peripheral collisions resembles qualitatively the $p+p$ distributions of Fig. 1, while the central S+S distribution is much flatter. The Λ and $\bar{\Lambda}$ yields for peripheral S+S collisions are too low to have any detectable influence on the shape of the dn/dy distribution (see Table III lower part).

The resulting $\langle \delta y \rangle$ values for symmetric $A+A$ collisions are shown in the middle part of Table IV, together with the multiplicities derived by summing $(dn/dy)\Delta y$ from y_m to $\approx y_p$. The Au+Au data have been extrapolated from the last measured point at $y=1.35$ to midrapidity at 1.60 by assuming a constant dn/dy, and from the lowest y point at 0.50 to $y=0$ by a straight line ending at $dn/dy=0$. The Si+Al and S+S points were extrapolated to $y=0$ following the same straight line recipe. These extrapolations follow the same procedures as were used for $p+p$ above.

It is possible to check the consistency of the calorimeter $\langle N_p^{\rm part} \rangle$ values of Table V against the summed $(dn/dy)\Delta y$ multiplicities. For Au+Au central collisions $\langle N_p^{\rm part} \rangle = 177.5$ corresponding to 71 protons which agrees well with the $\langle p \rangle = 70\pm1$ value of Table IV. For the central Si+Al and S+S the agreements are within approximately one particle, and there is full agreement for the peripheral collisions. This is very satisfactory.

The $\langle \delta y \rangle$ values for peripheral $A+A$ collisions are slightly larger than for $p+p$, while the central triggers $\langle \delta y \rangle$ for Au+Au and for Si+Al are significantly higher and the central S+S value is about twice the $p+p$ result.

C. Asymmetric A_1+A_2 collisions

If the average rapidity loss in an asymmetric collision is small one would expect to find a peak in the baryon dn/dy distribution at a rapidity somewhat below the projectile rapidity. At larger average rapidity losses the centroid of the

TABLE V. Trigger conditions and $\langle N_p^{\rm part} \rangle$ for A_1+A_2 collisions. The table shows the trigger conditions on centrality as explained in the text. The names in the column "Trigger" are used in the text to characterize the trigger conditions. The $\langle N_p^{\rm part} \rangle$ value given in square brackets is estimated, rather than measured, as explained in the text.

System	p_p (lab) A GeV/c	$\sigma_{\rm trig}/\sigma_{\rm inel}$ %	$\langle N_p^{\rm part} \rangle$	Trigger	Refs.
Au+Au	11.6	4	177.5	cent-4	[8,9]
Si+Al	14.6	58	4.1	periph	[12,26]
		7	23.7	cent-7	
		2	25.0	cent-2	
S+S	200.0		6.0	periph	[16]
		11	20.0	cent-T	
		3	26.0	cent-3	[17,28]
Si+Au	14.6	7	27.3	cent-7	[12]
		2	[27.6]	cent-2	

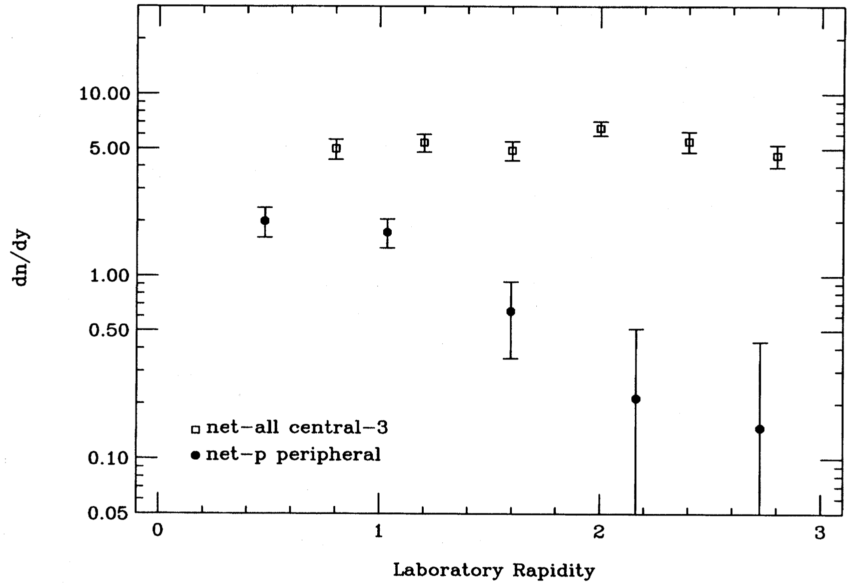

FIG. 3. Net baryon dn/dy for central (3%) and peripheral S+S collisions at 200A GeV/c. The trigger conditions are documented in Table V which also gives references for the data.

projectilelike peak will come at lower rapidity and the distribution would be expected to broaden and maybe start to overlap with the broadened distribution from the target baryons. For a situation where the overlap of target and projectile baryons is small, it is reasonable to define $\langle \delta y \rangle$ from Eq. (2) as the average rapidity of the high rapidity part of the baryon dn/dy distribution from $\approx y_p$ to a rapidity such that the integral under the distribution equals $\langle N_p^{\rm part} \rangle$. When the projectile and target nucleons mix strongly, the measurement of a net baryon dn/dy distribution does not suffice to define what should be taken as "projectile baryons;" additional measurements of, e.g., the proton to neutron ratio are required. A second possibility is to obtain guidance from a model of the collision, as is possible at Alternating Gradient Synchroton (AGS) energies from the work of Schlagel, Kahana, and Pang [27]. The data required, anyway, must cover the high rapidities well.

There are two asymmetric collision systems that have been studied in sufficient detail, that they can be used in combination in such an analysis, namely, Si+Au [12] and Si+Pb [13,14] at 14.6A GeV/c beam momentum (y_p=3.44). Figure 4 shows the Si+Au proton dn/dy up to y=2.1 paired with Si+Pb results for $y \geqslant 2.3$. The filled symbols represent data from charged multiplicity triggers corresponding to the highest multiplicities with a cross section of 7% of $\sigma_{\rm inel}$ for Si+Au and 8.6% for Si+Pb. The two data sets join smoothly in the region near y=2.2. The open symbols for Si+Au are from triggers with charged multiplicities above a threshold

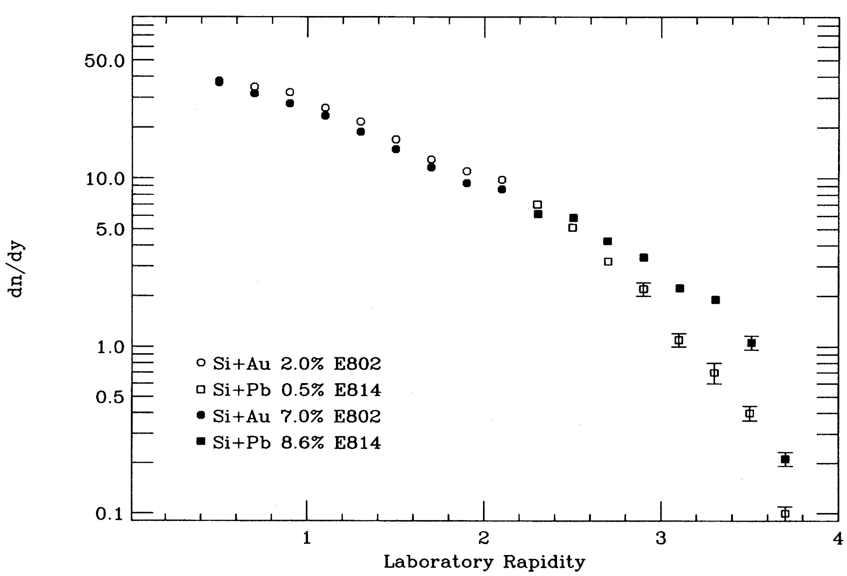

FIG. 4. Proton dn/dy plotted versus laboratory rapidity for Si+Au collisions (octagons) and Si+Pb reactions (squares). The open symbols correspond to a $\approx$7% centrality trigger and the filled symbols to a $\approx$2% centrality trigger. The Au data are from Ref. [12] and the Pb data from Refs. [13,14]. The figure is further explained in the text.

and corresponding to a cross section of 2% of $\sigma_{\rm inel}$. The Si+Pb data used a charged multiplicity trigger in a window corresponding to 0.5% of the inelastic cross section. The upper limit of the window is not at the maximum of the measured multiplicities, but close to it [14]. This particular pairing of data sets again join smoothly near $y=2.2$ and the data sets in fact agree within statistical errors in the overlap region $1.5\leq y\leq 2.1$ (the overlaps are not shown in the figure). The 0.007% or 2.8% data sets in[14] could equally well have been used in the rapidity region above $y=2.2$ and would lead to nearly identical results. It may be noted that the data include most of the protons from Λ decays.

For the 7% central Si+Au trigger, the calorimeter data (Table V) show that on the average there are 27.3 projectile participants. If we assume that there is little mixing of projectile and target baryons, a reasonable procedure in determining $\langle \delta y\rangle$ would be to use $\langle y_b\rangle$ evaluated from the proton dn/dy distribution from $y\approx 3.7$ to a rapidity $y_{\rm low}$, where the integral under the distribution is $\langle p\rangle=\frac{1}{2}27.3=13.65$, i.e., to $y_{\rm low}=1.51$. The resulting $\langle \delta y\rangle$ is given in Table IV.

The $\langle p\rangle/\langle n\rangle$ ratio has been measured for the Si+Pb system at $p_t=0$ and the 8.6% trigger [29]. It is quite constant from $y=2.1$ to 3.1, above which it fluctuates. The ratio has not been measured below $y=2$. A representative value for the rapidity range is $\langle p\rangle/\langle n\rangle=1/1.36$. If the assumption of small projectile target mixing is kept and the value 1/1.36 is taken for the rapidity range of interest here, the value of $\langle N_p^{\rm proj}\rangle=27.3$ is reached for $\langle p\rangle=27.3/2.36=11.6$. The corresponding range of rapidities in the integration is from ≈ 3.7 to $y_{\rm low}=1.63$ and the corresponding $\langle \delta y\rangle$ value (see Table IV) is 1.22, only slightly smaller than $\langle \delta y\rangle=1.33$ found for the $\langle p\rangle/\langle n\rangle=1$ recipe above. Conversely, the $\langle p\rangle/\langle n\rangle$ ratio may be taken as a measure of the projectile ($\langle p\rangle/\langle n\rangle=1.0$) and target ($\langle p\rangle/\langle n\rangle=82/126=1/1.54$) mixing, in which case the measured ratio indicates a ratio of 70% targetlike and 30% projectilelike nucleons. If this represents the true mixing over the rapidity interval below 3.1, the value of 13.65 projectile protons is not reached until $y=0.5$ with a $\langle \delta y\rangle\approx 2.1$ as a consequence, surely an upper limit.

The guidance from the cascade model calculations [27] favors the simple recipe of integrating the measured proton dn/dy distribution until the number of projectile proton participants is reached, because the model predicts rather little projectile-target baryon mixing, finding ten projectile protons above midrapidity.

There is no published value for $\langle N_p^{\rm part}\rangle$ corresponding to the 2% trigger condition. The value $\langle N_p^{\rm part}\rangle=27.6$ has been adopted from the results and calorimeter spectrum in Ref. [26]. The $\langle p\rangle$ and $\langle \delta y\rangle$ values for the two $\langle p\rangle/\langle n\rangle$ ratios are shown in Table IV for the small mixing assumption; both are slightly larger than the corresponding numbers from the 7% trigger (cent-7) as is expected from the more central trigger condition (see also Fig. 4).

At $200A$ GeV/c the S+Au data [18] cover the forward rapidities quite well, but not the rapidities near a $y_{\rm low}$ corresponding an integral over dn/dy of ≈ 16. It is in fact necessary to extrapolate the data in both the $y_{\rm low}$ and y_p regions, most seriously in the former. A tentative $\langle \delta y\rangle$ value from these data is from 2.0 (Λ's included) to 2.3 (no Λ's) with smooth (but arbitrary) extrapolations and unknown uncertainties. The trigger condition was 6% of $\sigma_{\rm inel}$ selected by a calorimeter threshold, $\langle p\rangle=16$, and the $\langle p\rangle/\langle n\rangle$ ratio assumed to be unity.

III. MIDRAPIDITY STACKING OF BARYONS

The center of the rapidity interval designated as "midrapidity" is defined as the maximum of the dn/dy distribution for K^- mesons at the AGS projectile momenta ($11.6A$ or $14.6A$ GeV/c) and $\bar{\Lambda}$ at the Super Proton Synchroton (SPS) beam momentum. The K^- data are often poor so the definition of the center must also use the K^+ results. The width of the midrapidity interval stretches from the center value up to where the dn/dy reaches half maximum and downwards the same amount. The width at AGS conditions turns out to be 1.20 in all cases, and it is 2.00 for SPS data. The center value varies in a systematic way with the collision system (see Table VI).

Since the baryon number is conserved, the initial number of baryons in the collision system defines a rigorous limit that cannot be exceeded. Not all of the initial baryons become participants in the collision, and a more reasonable sum rule limit should count only possible participants. A simple prescription for central heavy ion collisions is provided by the geometrical fireball for zero impact parameter. Here the participant volume of the larger collision partner, the target, is the volume of a cylinder cut along a target diameter with a radius equal to that of the projectile plus the volumes of the two spherical segments at the ends of the cylinder. The participant volume of the projectile is its volume (at rest). Assuming the volumes of target and projectile to be given by

$$V=\frac{4\pi}{3}\, r_0^3 A \tag{9}$$

with the same value of r_0 for all cases considered, the sum rule for baryons is

$$\langle n_b\rangle=A_1+A_2-(A_2^{2/3}-A_1^{2/3})^{3/2} \tag{10}$$

and the corresponding one for protons

$$\langle n_{\rm prot}\rangle=Z_1+Z_2-Z_2[1-(A_1/A_2)^{2/3}]^{3/2}. \tag{11}$$

Here the projectile has A_1 baryons and Z_1 protons and the target A_2 and Z_2, respectively. The sum rules for central $A+A$ collisions just equal the the initial number of baryons or protons. The proton rule is of course not a strict sum rule, since the net number of protons after the collision may not equal the number before. The rule is used here because the neutrons and antineutrons have not been measured, so the baryon rule becomes more and more irrelevant as the collision systems become heavier, with higher and higher initial neutron excess. The multiplicities Δ_m and the corresponding fractions F_b of multiplicity divided by the sum rule are collected in Table VI. No sum rule analysis was made for the peripheral heavy ion collisions.

For $p+A$ processes we have used the results of the wounded nucleon model as the sum-rule limit. The model is described in [30] and the results quoted in Table VII are impact parameter averaged, and thus match the minimum bias trigger condition of the data in Ref. [11]. The leftmost

TABLE VI. Sum-rule fractions for midrapidity baryons. The table shows the results of the analysis of midrapidity stacking. The columns named y_1 and y_2 state the rapidity interval used, and the next column marked Δ_m gives the multiplicity found in the rapidity interval. The particle of the analysis is given in the next column, and the sum-rule fractions F_b for the baryon and proton sum rules follow next. No errors have been assigned to the F_b values, although the statistical relative errors would be identical to those of the Δ_m column. The final column shows the trigger conditions of the experiment; see also Table V.

System	p_p A GeV/c	y_1	y_2	Δ_m	Particle	Fraction F_b		Trigger
						bar	prot	
Au+Au	11.6	1.0	2.2	74.40±0.80	prot	0.19	0.47	cent-4
$p+p$	14.6	1.1	2.3	0.34±0.01	prot	0.17	0.17	min
p+Be		1.1	2.3	0.33±0.03	prot	0.13	0.19	min
p+Al		1.1	2.3	0.40±0.01	prot	0.13	0.20	min
p+Cu		1.0	2.2	0.50±0.01	prot	0.14	0.23	min
p+Au		0.9	2.1	0.59±0.01	prot	0.13	0.24	min
Si+Al		1.1	2.3	8.55±0.08	prot	0.16	0.32	cent-7
Si+Cu		0.9	2.1	11.67±0.14	prot	0.16	0.39	cent-7
Si+Au		0.7	1.9	26.61±0.26	prot	0.26	0.60	cent-2
		0.7	1.9	23.43±0.15	prot	0.23	0.53	cent-7
$p+p$	200.0	2.0	4.0	0.20±0.02	prot	0.10	0.10	min
		2.0	4.0	0.20±0.02	net all	0.10	0.10	min
S+S		2.0	4.0	10.70±0.60	net all	0.17	0.33	cent-3

column in the table shows the sum rule limits for baryons. The proton numbers were derived by taking the target $\langle p\rangle/\langle n\rangle$ ratio into account. For $p+p$ collisions the baryon and proton sum rules are both equal to 2. The final results for Δ_m and F_b are given in Table VI. From the extrapolated 200 GeV/c p+Pb "central" data quoted in Ref. [5] an F_b value of ≈0.24 may be derived, a value close to the p+Au 14.6 GeV/c number in the table.

IV. SYSTEMATICS AND DISCUSSION

A. Average rapidity losses

The systematic trends for the average rapidity loss are apparent from Table IV. At a given beam momentum, $\langle \delta y\rangle$ for peripheral $A+A$ collisions agree with the corresponding $p+p$ values. For $A+A$ collisions $\langle \delta y\rangle$ increases with centrality. For $p+p$ and $A+A$ the average rapidity loss increases with beam rapidity. In the $p+p$ case $\langle \delta y\rangle$ does not scale with y_p, but for the comparisons of Si+Al to S+S and Si+Au to S+Au central collisions $\langle \delta y\rangle$ does scale with beam rapidity. Finally, for a gold target, the central asymmetric collision (Si+Au) has a larger average rapidity loss than the central symmetric (Au+Au) collision. The largest value of $\langle \delta y\rangle$ seems to ensue for S+Au, central trigger, at a beam momentum of 200A GeV/c.

TABLE VII. Sum rule values for $p+A$ reactions. Column 2 of the table shows the number of baryon participants in $p+A$ collisions calculated from the wounded nucleon model [30]. The calculation was averaged over impact parameters to imitate the minimum bias trigger condition of the experiment. The third column gives the corresponding number of protons. For further details see the text.

System	Baryons	Protons
p+Be	2.5	1.7
p+Al	3.0	2.0
p+Cu	3.6	2.2
p+Au	4.7	2.5

The average rapidity losses shown in Table IV are not sensitive to the various prescriptions applied, protons, net protons, net all, or different divisions between target and projectile related protons. It is emphasized that the quoted values of the average rapidity loss are lower limits. This is particularly true for the low energy data where it is fairly easy for target baryons to reach rapidities above midrapidity and thus be included in the calculation of the projectile baryon rapidity loss. To what degree this happens, as discussed above, cannot be established from the data alone. Thus the observation of approximate y_p scaling of the distributions in $A+A$ reactions might be coincidental. It could be argued that $\langle \delta y\rangle$ for the $A+A$ collisions should follow the weak increase with y_p observed in $p+p$ if $A+A$ stopping is built solely on independent multiple elementary collisions. In addition there are, however, the effects of resonance excitation and rescattering which modify the simple picture.

The observation of a larger $\langle \delta y\rangle$ for Si+Au than for Au+Au at AGS energies can be attributed to the following. In central Si+Au collisions all the incident baryons from the smaller Si projectile see nearly the full diameter of the Au target for a range of impact parameters and thus have the possibility of undergoing many collisions and slowing down; in central Au+Au collisions, on the other hand, full overlap only happens for zero impact parameter with no cross section and a sizeable fraction of the incident baryons for finite impact parameters do not overlap with any of the target baryons or only with a few and thus do not contribute much to the stopping, thereby reducing the average rapidity loss.

It may finally be noted that there is a dramatic difference in the shapes of the dn/dy distributions when going from the $p+p$ system over, e.g., Si+Al, to Au+Au: the prominent projectile and target peaks in $p+p$ (see Fig. 1) have totally disappeared in Au+Au.

B. Midrapidity stacking

The ratio F_b is a measure of the opacity of the collision system. A small value of F_b indicates transparency. The F_b values in Table VI are sensitive to the recipe used, in particular to the rapidity interval used for determining Δ_m, so it is not clear what value to expect for a completely black system. If the rapidity interval used in the integrations is increased by 0.1, the Δ_m and hence the F_b increase by $\approx 10\%$ for most of the systems considered. For Si+Au, if the integration interval is moved by 0.1 towards lower (higher) rapidities, F_b increases (decreases) by $\approx 10\%$. The largest F_b values are encountered for protons (rather than baryons), and the maximum value of 0.60 is for Si+Au, the cent-2 trigger. This value may well indicate blackness, and with a small modification of the integration recipe it might have been 0.7 or 0.5. The proton F_b systematics of Table VI may be summarized as follows: the systems Au+Au and Si+Au have the highest opacities; Si+Cu, Si+Al, and S+S form an intermediate group, while $p+p$ and $p+A$ constitute the third group with the lowest F_b values.

If the S+Au central collision net all data of Ref. [18] are extrapolated smoothly (but arbitrarily) to smaller rapidities a proton F_b value of ≈ 0.5 obtains. It therefore seems possible to conclude that, for the available data, opacity increases with the size of the system, but is, for a given size system, largely independent of the projectile momentum.

The systematics for the baryon F_b values are less clear. The largest values still ensue for Si+Au, while the remainder of the collision systems cluster around the 14.6 GeV/c $p+p$ result, with one exception, $p+p$ at 200 GeV/c which has a much lower value. We take this lack of clear trends to reflect mainly that a sum rule which includes neutrons is being used on data where neutrons were not observed.

C. Concluding remarks

In the incident momentum range from 11.6A to 200A GeV/c studied here the $\langle \delta y \rangle$ and proton F_b values are correlated: if $\langle \delta y \rangle$ for one collision system is larger than $\langle \delta y \rangle$ for some other system, the F_b values for the systems have the same relation. We take that to be characteristic of collisions with a high degree of opacity. At much higher incident momenta a net-baryon-free midrapidity region may develop (Bjorken regime), in which case F_b will go towards zero, while $\langle \delta y \rangle$ will still be large and the correlation between the two measures will be broken.

The new Pb beam studies at the SPS are at a beam rapidity between the AGS and SPS rapidities studied here. Based on the systematics presented here a $\langle \delta y \rangle$ value of ≈ 1.8 is expected from y scaling of the Au+Au result and a proton F_b value near 0.5 is predicted for central collisions. If the systematics of the present analysis hold true at higher bombarding energies, $\langle \delta y \rangle$ for central Au+Au reactions at the future Relativistic Heavy Ion Collider (RHIC), with $y_p = 10.7$, will be ≈ 3.4 and the proton F_b should come near 0.5, a prediction that is subject to the assumption of high opacity. The prediction of $\langle \delta y \rangle$ from the relativistic quantum molecular model (RQMD) model [31] for central Au+Au collisions at RHIC energies is 2.6 and the predicted F_b value is ≈ 0.3 counting all net baryons. The RQMD model thus predicts a decrease in opacity and breakage of the of rapidity scaling for $\langle \delta y \rangle$.

ACKNOWLEDGMENTS

The authors would like to thank Dr. I. Mishustin and Dr. J. J. Gårdhøje for valuable comments. One of the authors (O.H.) is indebted to the direktør Ib Henriksen Foundation for a grant. This work was supported in part by the U.S. Department of Energy under Contract No. DE-AC02-76CH00016 with Brookhaven National Laboratory and in part by the Science Research Council of Denmark.

[1] N. Bohr, Philos. Mag. **25**, 10 (1913).
[2] N. Bohr, Philos. Mag. **30**, 581 (1915).
[3] Aa. Bohr, K. Dan. Vidensk. Selsk. Mat. Fys. Medd. **24**, No. 19 (1948).
[4] S. Daté, M. Gyulassy, and H. Sumiyoshi, Phys. Rev. D **32**, 619 (1985).
[5] W. Busza and R. Ledoux, Annu. Rev. Nucl. Part. Sci. **38**, 119 (1988).
[6] M. Jacob, Nucl. Phys. **A418**, 7c (1983).
[7] E. V. Shuryak, Phys. Rep. **61**, 71 (1980).
[8] M. Gonin, Nucl. Phys. **A566**, 601c (1994).
[9] F. Videbæk, in "HIPAGS," edited by G. Stephans *et al.*, Report No. MITLNS-2158, 1993, p. 89.
[10] V. Blobel *et al.*, Nucl. Phys. **B69**, 454 (1974).
[11] E802 Collaboration, T. Abbott *et al.*, Phys. Rev. D **45**, 3906 (1992).
[12] E802 Collaboration, T. Abbott *et al.*, Phys. Rev. C **50**, 1024 (1994).
[13] E814 Collaboration, J. Barrette *et al.*, Z. Phys. C **59**, 211 (1993).
[14] E814 Collaboration, J. Barrette *et al.*, Phys. Rev. C **50**, 3047 (1994).
[15] V. V. Ammosov *et al.*, Nuovo Cimento A **40**, No. 3, 237 (1977).
[16] NA35 Collaboration, J. Bächler *et al.*, Phys. Rev. Lett. **72**, 1419 (1994).
[17] NA35 Collaboration, A. Bartke *et al.*, Z. Phys. C **48**, 191 (1990).
[18] NA35 Collaboration, D. Röhrich *et al.*, Nucl. Phys. A **566**, 35c (1994).
[19] K. Jaeger *et al.*, Phys. Rev. D **11**, 2405 (1975).
[20] F. LoPinto *et al.*, Phys. Rev. D **22**, 573 (1980).
[21] M. Aguilar-Benitz *et al.*, Z. Phys. C **50**, 405 (1991).
[22] M. Gazdzicki and O. Hansen, Nucl. Phys. **A528**, 754 (1991).
[23] E. Stenlund and I. Otterlund, Report No. CERN-EP/82-42, 1982.
[24] A. Wroblewski, in Proceedings of the International Symposium on Multiparticle Dynamics, Kayserberg, 1977, A1 (unpublished).
[25] H. Bøggild and T. Ferbel, Annu. Rev. Nucl. Sci. **24**, 451 (1974) (Fig. 28).

[26] E802 Collaboration, T. Abbott *et al.*, Phys. Lett. B **291**, 341 (1992).
[27] T. J. Schlagel, S. H. Kahana, and Y. Pang, Phys. Rev. Lett. **69**, 3290 (1992).
[28] NA35 Collaboration, T. Alber *et al.*, Nucl. Phys. **A566**, 35c (1994).
[29] E814 Collaboration, J. Barette *et al.*, Phys. Rev. C **45**, 819 (1992).
[30] H. Brody *et al.*, Phys. Rev. D **28**, 2334 (1983).
[31] Th. Schönfeld *et al.*, Mod. Phys. Lett. A **28**, 2631 (1993).